RECENT PROGRESS ON CLOUD-RESOLVING MODELING OF TOGA COARE AND GATE CLOUD SYSTEMS

Xiaoqing Wu and Mitchell W. Moncrieff
National Center for Atmospheric Research
Boulder, CO 80307, USA

Abstract

The cloud-resolving modeling (CRM) approach is used to simulate the TOGA COARE and GATE cloud systems. The objective is to give insight into two important questions regarding (1) the use of CRM for the improvement of parameterization of cloud systems in large-scale models, and (2) the importance of three-dimensional (3D) CRMs.

Two 39-day two-dimensional (2D) simulations are performed from December 5, 1992 through January 12, 1993 during TOGA COARE. A cloud-scale model, combined with cloud-interactive radiation scheme, was driven by the observed *evolving* large-scale forcing for the temperature and moisture, *evolving* large-scale horizontal winds, and *evolving* sea surface temperature, all representing conditions averaged over the Intensive Flux Array of TOGA COARE. The CRM-produced data generally compare well with the observational data and can be used to examine interactions of the simulated cloud systems with radiative and surface processes. However, the dearth of observed data to specify large-scale forcing for the condensed water, combined with the use of periodic lateral boundary conditions, resulted in an unrealistically enhanced moisture in the upper troposphere.

The preliminary analyses of 7-day three-dimensional simulation of GATE cloud systems (from September 1 through 7, 1974) indicate that the 3D framework is important regarding the response of cloud systems to the large-scale forcing, especially when the dynamical factors such as the low-level vertical wind shear are present. Transitions among regimes occurred spontaneously as the large-scale condition evolved. This supports that the vertical wind shear is an important factor in formulating the relationship between large-scale variables and collective effects of cloud systems for parameterization purposes.

1. INTRODUCTION

It is well known that the representation of cloud systems in atmospheric general circulation models (GCMs) contains great uncertainty. Cess et al. (1989) intercompared 14 GCMs and found that the cloud-climate feedback produced by GCMs is different ranging from modest negative to strong positive feedback. This pointed to the need for improvements in the representation of cloud systems in GCMs. Recently, another intercomparison project using 15 GCMs shows that no GCM has produced the major signal of the intraseasonal oscillation as identified in observational analyses (Slingo et al., 1996). The accurate representation of cloud systems in GCMs will help the understanding of the interaction between clouds and radiation, the role of moisture in the atmospheric energy cycle, and the role of tropical precipitating cloud systems in the coupling between ocean and atmosphere. Clearly, more efforts are required to

improve the physics of the convection parameterization schemes and to formulate the relationship between large-scale dynamics and sub-grid-scale cloud processes with less empirical tuning of parameters in the schemes (e.g., Browning, 1994).

The obvious question is what can we do to make progress on this complicated nonlinear problem? The sensitivity tests of parameterization schemes in GCMs is one way but with a limitation. Since convection is not only the process be parameterized in GCMs, the indirect interaction between convection and other processes such as microphysics, radiation and surface fluxes makes the interpretation of results difficult. Observational, diagnostic, semi-prognostic, and theoretical studies have investigated various aspects of cloud-large-scale interaction and made significant progress over the past three decades (see references in Grabowski et al., 1996 and Wu et al., 1996). Recognizing the lack of cloud-scale data, the cloud-resolving modeling (CRM) approach has been developed and used to analyze the statistical properties and dynamical processes of cloud systems. In the previous studies of using CRM approach, the cloud-scale models were either forced by a constant forcing or highly idealized evolving forcing. Although this approach can help understand some basic mechanisms and processes associated with organized convection, the limitation here is that the quantitative comparison between models and observations is impossible.

To fully explore the advantage of the CRM approach, we use the *evolving* large-scale forcing, the *evolving* large-scale wind field, and the *evolving* sea surface temperature (SST) determined from observational analyses (Grabowski et al., 1996 and Wu et al., 1996). The motivation is to produce realizations of tropical cloud systems and realistic cloud-scale datasets over climatically key areas over a long period. A CRM approach that combines evolving large-scale observations with the cloud-scale model allows the *quantitative* comparison between models and observations. With this kind of experiment design, the intercomparison among different cloud-scale models can be performed to evaluate the sensitivity of *explicitly-simulated* cloud properties to the microphysics, radiation, and surface processes which are mostly different among models (Moncrieff et al., 1997). The direct link between CRM and GCM can be established using the verified cloud-scale data.

In the following sections of this paper, the experimental design of the CRM will be summarized in section 2. Readers can find the detail description of the method in Grabowski et al. (1996) and Wu et al. (1996). Section 3 will present 39-day two-dimensional (2D) simulations of TOGA COARE (the Tropical Ocean Global Atmosphere (TOGA) Coupled Ocean Atmosphere Response Experiment) cloud systems and the comparison with observations, which is the focus of this paper. With the development of parallel code of Clark-Hall cloud model (Clark

et al., 1996; Hall and Clark, 1996) that is used in the CRM approach, a three-dimensional (3D) simulation of GATE (the Global Atmospheric Research Programme Atlantic Tropical Experiment) cloud systems with a large domain now can be performed for a week-long period. Preliminary analyses from the 3D simulation will be given in section 4. Finally the major finding will be listed in section 5.

2. CRM APPROACH

The major part of the CRM approach is the cloud-scale model, which is the Clark-Hall anelastic cloud model (Clark et al., 1996) in this study. The cloud-scale dynamics are fully resolved in the model. The microphysical processes are parameterized by the Kessler (1969) bulk warm rain scheme and the Koenig and Murray (1976) bulk ice scheme. The direct interaction between clouds and radiative processes occurs through the coupling of NCAR's Community Climate Model 2 (CCM2) radiation model (Kiehl et al., 1994) with the cloud-scale model. The surface heat fluxes are calculated by a simplified version of the TOGA COARE surface flux algorithm (Fairall et al., 1996).

The evolving large-scale tendencies are added to the temperature and moisture conservation equations. Since the large-scale forcing for the horizontal wind field (especially the large-scale pressure gradient) is difficult to obtain from observations, a relaxation term is included in the momentum equations. This is the simplest way to emulate the control of the cloud system dynamics by the observed large-scale momentum and shear. The domain-averaged horizontal velocities are thereby constrained to follow the observed values. A detailed discussion of the way a cloud model is forced by observed evolving large-scale conditions is presented in Grabowski et al. (1996) and Wu et al. (1996).

2.1 Two-dimensional experiment design

For 2D simulations, the domain is 900 km long and 40 km deep with a 3-km horizontal resolution and a stretched grid in the vertical with 52 levels (100 m at the surface, increasing to 1500 m at the top of the domain). The model x-axis is aligned east-west in the two-dimensional $x - z$ frame. A time-step of 15 s is used. Free-slip, rigid bottom and top boundary conditions are applied together with a gravity wave absorber in the uppermost 14-km of the domain. Periodic lateral boundary conditions ensure that there is no forcing inside the domain apart from large-scale forcing. The Coriolis term in the model equations is set to zero (note the relaxation to the large-scale wind field implicitly includes the effects of planetary rotation). Radiation calculations are performed every 150 s while the most recent tendencies were applied between consecutive radiation calculations.

2.2 Three-dimensional experiment design

For 3D simulations, the horizontal domain is 400 km×400 km with a 2-km resolution. There are 42 levels in the vertical with a stretched grid (100 m at the surface, increasing to 1200 m at the top of the domain). The bottom, top and lateral boundary conditions are the same as the 2D setup. The radiation model was not coupled with the 3D run but the observed radiative tendency was included in the large-scale forcing.

3. TWO-DIMENSIONAL SIMULATIONS OF TOGA COARE CLOUD SYSTEMS

3.1 Large-scale forcing, wind field and SST

The objectively-analyzed TOGA COARE sounding data discussed in Lin and Johnson (1996a, b) were used. The evolving large-scale profiles of temperature, moisture, winds and advective tendencies of temperature and moisture were averaged over the Intensive Flux Array (IFA) of TOGA COARE from December 5, 1992 through January 12, 1993. The IFA domain measures about 700 km in the east-west direction (151°-158°E) and about 500 km south-north (4°S-1°N). The averaged SST data over the IFA was calculated from four buoy data sets; namely, the Improved METeorological surface mooring (IMET) and three TOGA TAO (Tropical Atmosphere Ocean) ATLAS (Automated Temperature Line Acquisition System) moorings.

Figure 1 shows the evolution of profiles of the large-scale forcing for the temperature and water vapor mixing ratio, the east-west wind component, and the SST averaged over the IFA during the 39-day period from December 5, 1992 through January 12, 1993. Several distinct features were observed during this period. Relatively weak winds and weak convection associated with episodes of weak large-scale cooling and moistening prevailed in the first six days (5 to 10 December), causing a warm SST and a strong diurnal cycle. Weak westerly winds across the entire troposphere gave way to easterlies toward the end of this period. During the period of 11-27 December, episodes of very strong cooling and moistening were present over the IFA and easterlies were slowly giving way to westerlies. The low-level wind shear was enhanced with the onset of westerly winds below 3 km. The SST was decreasing and the amplitude of the diurnal cycle was considerably smaller, apart from days 15, 18 and 19 when only a few clouds occurred in satellite pictures (not shown).

As the westerly winds increased to their maximum speed and depth (the period 27 December through 6 January), the magnitude and duration of the large-scale cooling and moistening were significantly decreased. As a result of strong low-level winds, the SST decreased at a rate of about 0.1 K day^{-1}, reaching a minimum on 5 January. The phase shift between the period of the maximum convection (11 through 24 December) and the period of the maximum westerly winds in the lower and middle troposphere (27 December through 6 January) is consistent with the

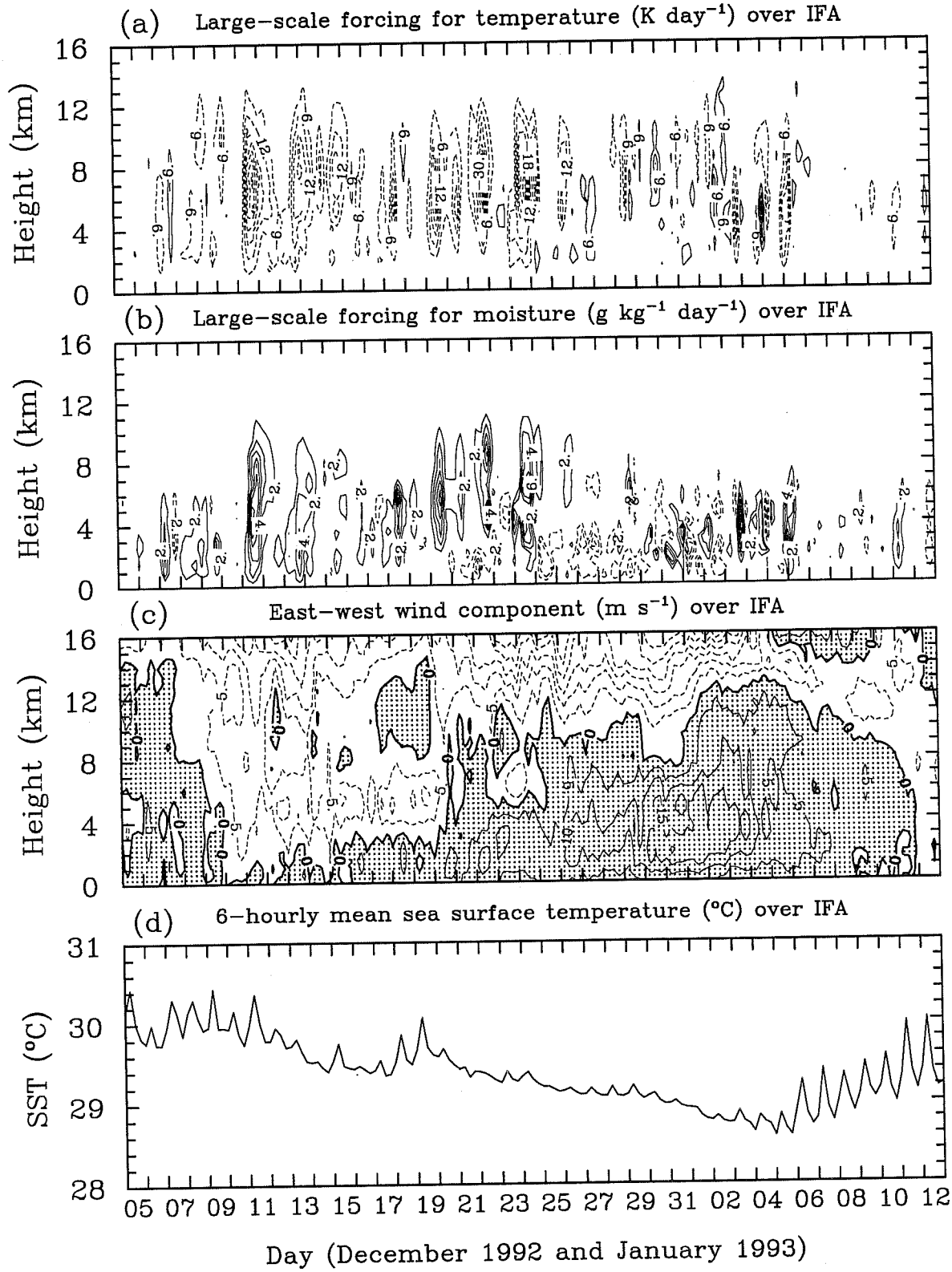

Figure 1: Evolution of the large-scale forcing for the temperature (panel a) and the water vapor mixing ratio (panel b), the east–west wind component (panel c), and the sea surface temperature (°C, panel d) averaged over the IFA for the 39–day period. Contour intervals are 6 K day^{-1} in (a), 2 g kg^{-1} day^{-1} in (b), and 5 m s^{-1} in (c).

discussion in Lin and Johnson (1996a). The westerlies gradually decreased in strength and only a few minor cooling and moistening episodes existed after 6 January. The SST subsequently started to warm and its diurnal cycle was correspondingly enhanced.

3.2 Evolution of temperature and moisture fields

Figure 2 shows profiles of the difference between model-produced and observed temperature, water vapor mixing ratio and relative humidity fields for the control experiment E0. The model-produced fields are averaged over the 900-km domain and a 6-hour period. With the experimental design presented in section 2, the agreement between model-produced and observed temperature and moisture fields is a necessary condition for evaluating model performance. The differences between model-produced and observed fields are generally small except during the periods when the forcing changes from strong to weak. The model-produced temperature is too warm in the upper levels (2 to 6 K higher than observations) during 1 through 12 January in Fig. 2a, and the moisture field is too moist (1 to 4 g kg^{-1} higher in water vapor mixing ratio and 25% higher in relative humidity) for 18 and 19 December and during 6 through 12 January in Figs. 2b and 2c.

The explanation for these differences is as follows. Since no large-scale forcing exists to control the condensed water, the ice water moves out one side of the domain but reenter from the other side due to the periodic lateral boundary conditions. This unrealistic storage process is particularly problematic when the forcing changes from strong to weak because the water condensed inside the domain should disappear by mean horizontal advection. Interaction of the accumulated ice water with radiation generates a greenhouse effect as shown in the period of 1 through 12 January. For the 18-19 December case, the ice-radiation interaction seems not to affect the temperature field since the period of weak forcing is relatively short and the strong forcing occurs after 19 December. Other possibilities for the differences between model-produced and observed moisture profiles (such as the accuracy of observed large-scale forcing and effects of the microphysical parameterizations) are not ruled out at this stage. It should be noted that the error after 6 January is not a manifestation of a purely numerically-generated bias associated with a long simulation.

To control the moisture, a relaxation term was added to the water vapor equation in an additional experiment E1 as a surrogate to horizontal advection out of the domain. The relaxation term is

$$\left(\frac{\partial q_v}{\partial t}\right)_{rel} = -\frac{\hat{q}_v - \overline{Q}_v}{\tau}, \tag{1}$$

where $\overline{Q}_v$ represents the observed large-scale water vapor mixing ratio, $\hat{q}_v$ is the model-predicted

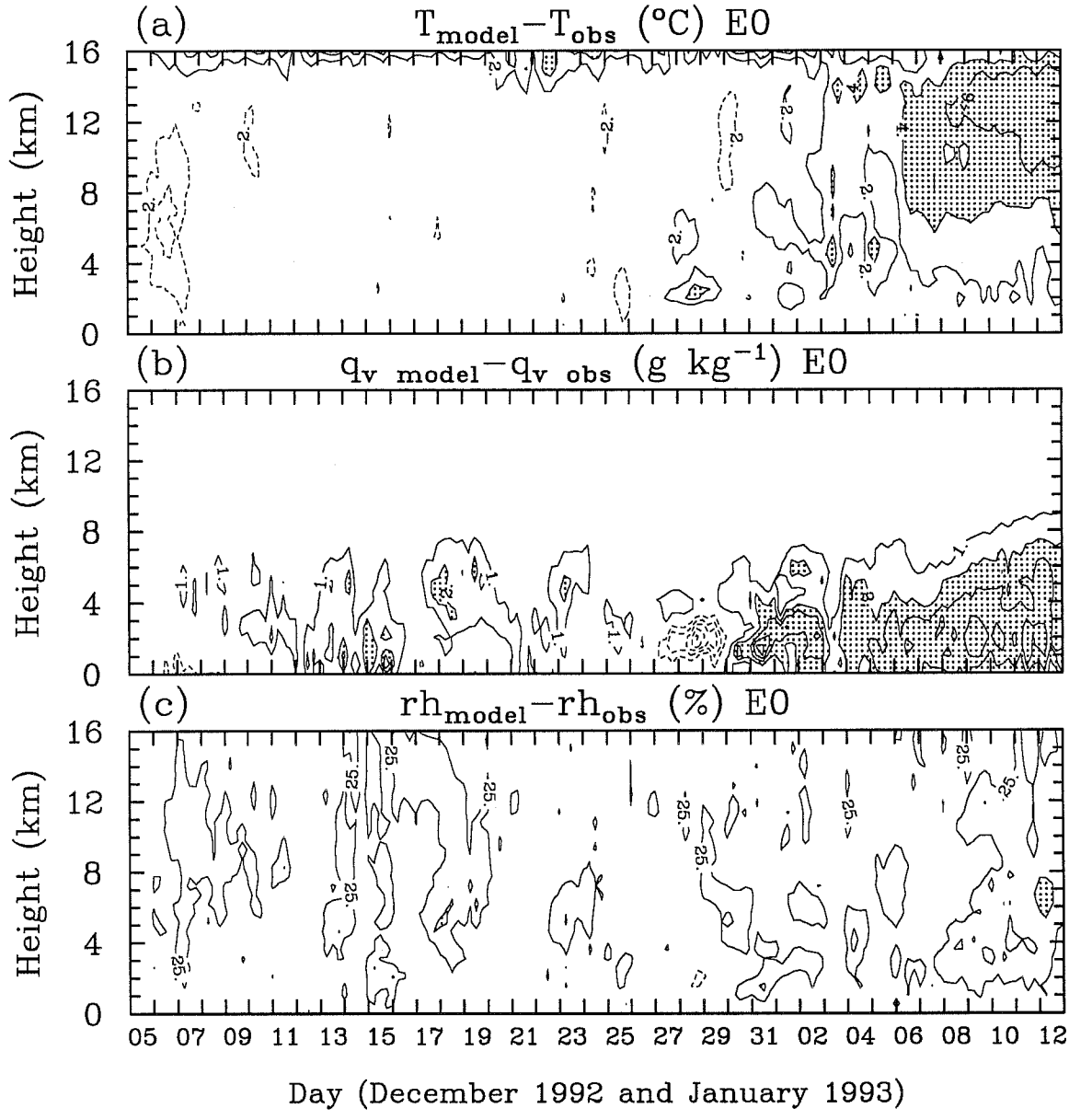

Figure 2: (a) Difference between model–produced and observed temperature (contour interval 2°C, the shading area is larger than 4°C), (b) ratio of moisture difference to model–produced water vapor mixing ratio (contour interval 25%, the shading area is larger than 50%) for the control experiment.

water vapor mixing ratio horizontally-averaged over the 900-km domain, and $\tau = 1$ day is the time scale selected based on moisture increase in the control experiment. Figure 3 shows the same fields as Fig. 2, except for the experiment E1 which applies the moisture relaxation technique. It is clear from Fig. 3 that the moisture field is greatly improved, and the better control of the upper tropospheric moisture greatly reduces the greenhouse effect in the temperature field. Although the technique applied is but a simple way to control the moisture during extended simulations, the results show importance of the appropriate moisture profiles to the production of realistic cloud systems.

3.3 Mean profiles of heat and moisture budgets

Consistency between the model-produced and observed heat and moisture budget residuals (Yanai et al., 1973) is a necessary condition for a satisfactory model performance. Figure 4 shows the 39-day mean profiles of observed and model-produced domain-averaged Q_1 and Q_2 for both experiments E0 and E1. Both experiments reproduce the observed Q_1 and Q_2 profiles fairly well. The small difference between model and observed Q_1 in the control experiment (Fig. 4a) is reduced in the experiment with the relaxation term. This is because better control of the moisture profile in the E1 experiment removes feedback that the enhanced moisture causes to the temperature field through the greenhouse effect (Fig. 4c). The Q_{2M} profiles (Figs. 4b and 4d) do not differ significantly in the upper troposphere despite application of the relaxation technique. This is consistent with the notion that the relaxation technique controls the upper tropospheric moisture by removing excess water vapor, rather than controling the cloud condensate. As a result, enhanced sublimation of the ice field, in response to the moisture sink associated with the relaxation technique, bring back a moisture residual in Q_{2M}.

3.4 Evolution of surface precipitation

Surface precipitation is a by-product of various physical processes in the CRM and is potentially important when CRMs are coupled with the ocean. Figure 5 shows the model-produced 6-hourly rainfall rates during the 39-day period for experiments E0 and E1, as well as the rainfall rates diagnosed from observations. The budget diagnosed rainfall rate is from Lin and Johnson (1996b) and is obtained by combining the vertically-integrated moisture budget residual (Q_2) and the observed surface latent heat flux. Model-produced rainfall rate is averaged over the 900-km domain and during the 6-hour period. Both model and budget-calculated rainfall rates show similar variations during the 39-day period. The 39-day means are nearly the same, 0.32 mm hr^{-1} from the experiment E0, 0.31 mm hr^{-1} from the experiment E1, and 0.35 mm hr^{-1} from the budget. Lin and Johnson (1996b) showed that the budget derived rainfall

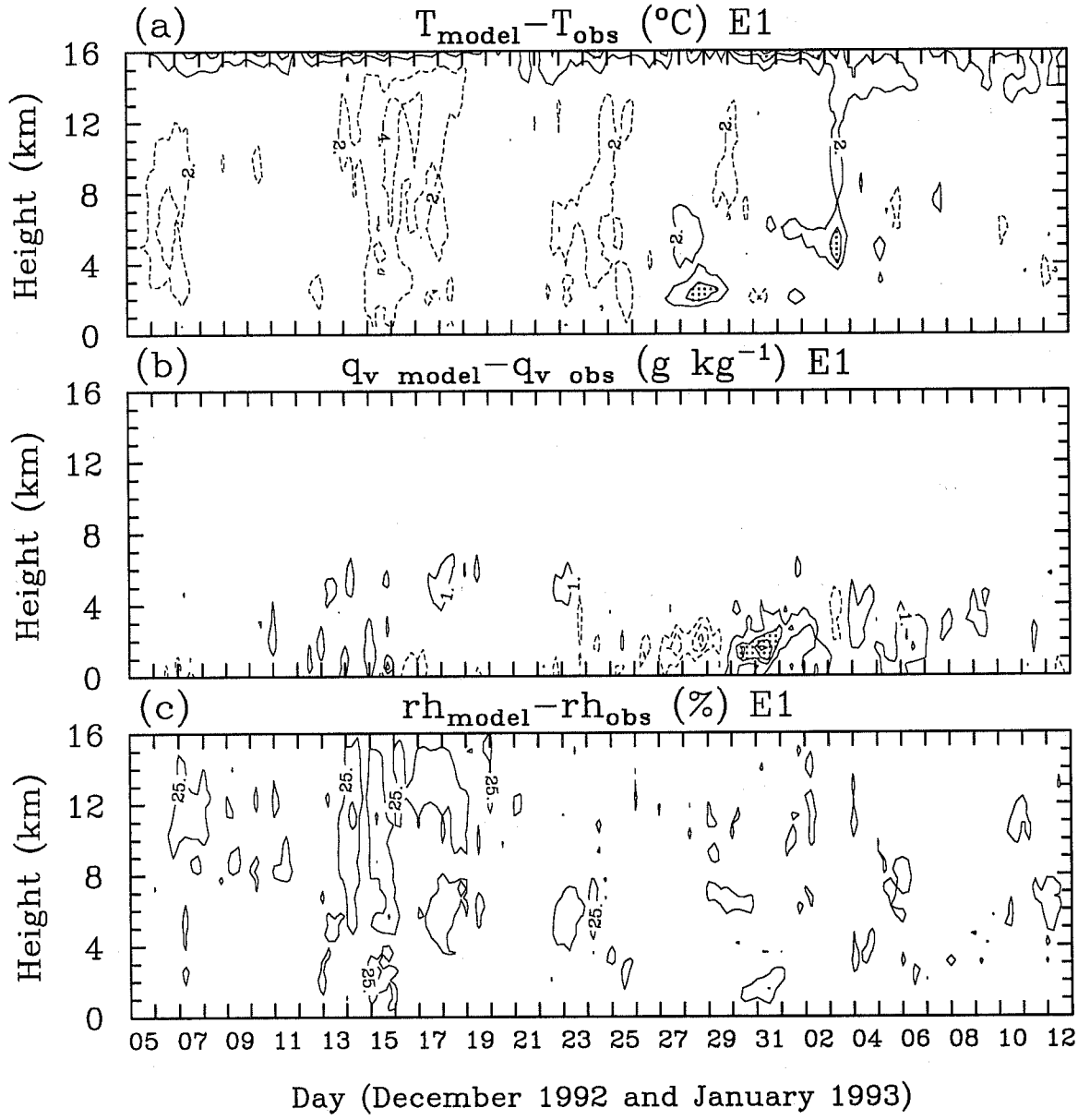

Figure 3: Same as Fig. 2 except for the experiment with the q_v relaxation term.

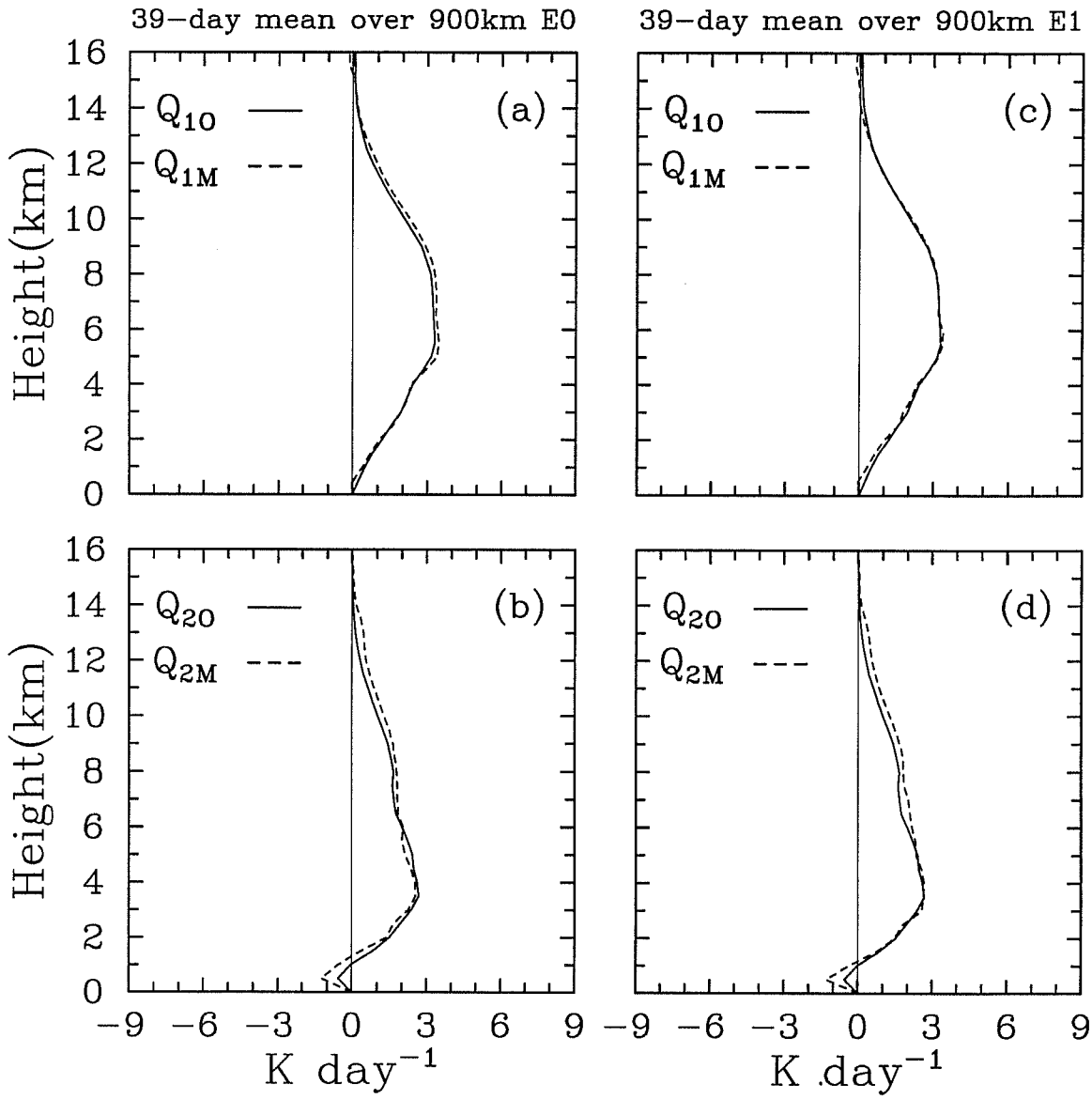

Figure 4: Profiles of the observed Q_{1O} (solid), the model–produced Q_{1M} (dashed), the observed Q_{2O} (solid) and the model–produced Q_{2M} (dashed) averaged over the 39–day period and 900–km domain for the experiment E0 (a, b) and the experiment E1 (c, d). Units are K day^{-1}.

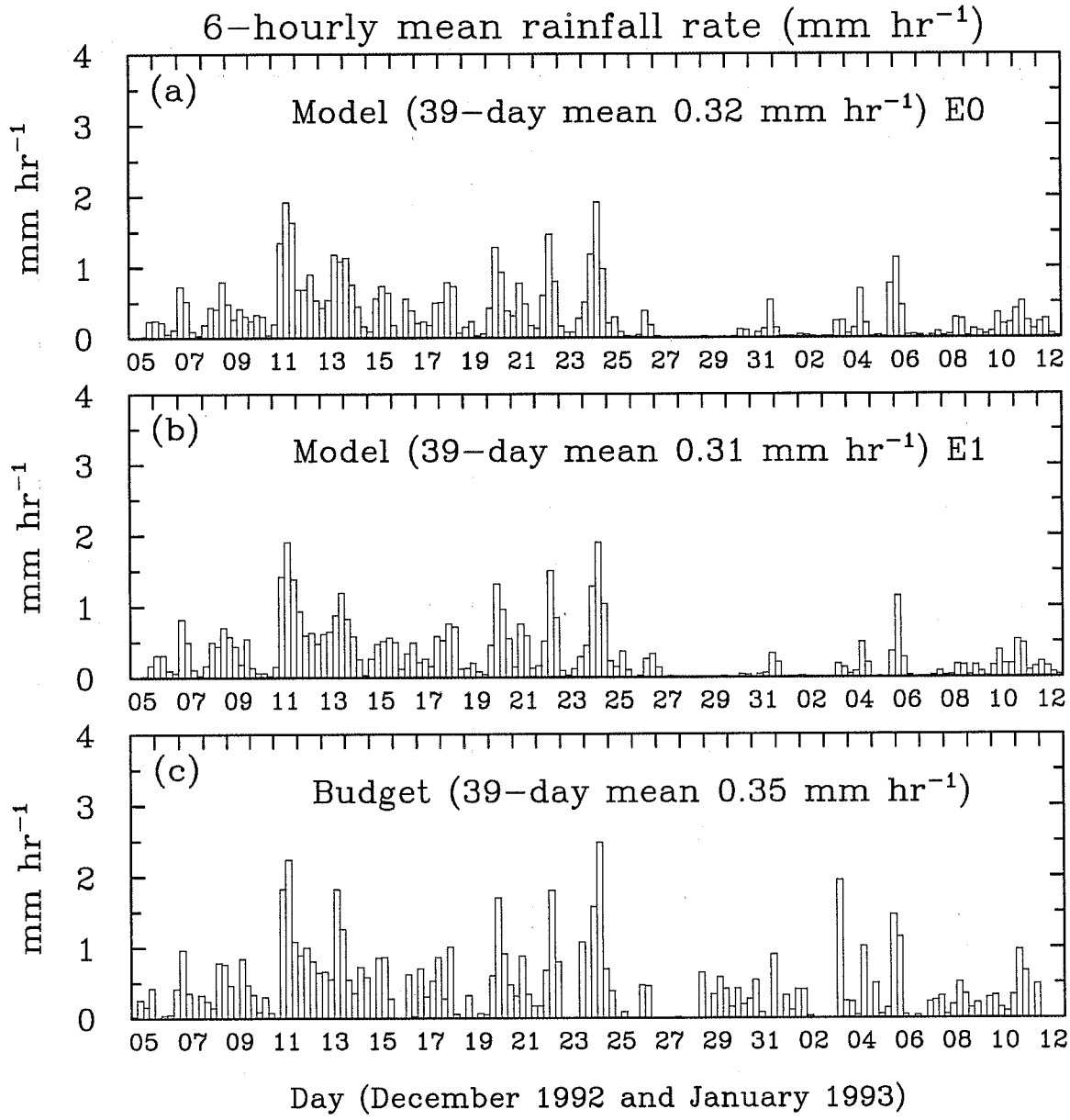

Figure 5: Figure 7. Evolution of the domain–averaged 6–hourly mean rainfall rates from (a) the experiment E0 and (b) the experiment E1, and (c) 6–hourly rainfall rates from the moisture budget and latent heat flux for the 39–day period.

rate agrees well with the rainfall rate independently-obtained from other observational sources such as DMSP Special Sensor Microwave/Imager (SSM/I).

3.5 Cloud mass fluxes

The cloud mass flux is an important quantity for the parameterization of cloud systems in large-scale models, and is a quantity which is impossible to observe especially over a large area. So field data does not exist to directly evaluate the model-produced cloud mass fluxes. Figure 6 presents time series of cloud mass fluxes from the experiment E1 averaged over regions where the total condensate mixing ratio is equal to or larger than 0.1 g kg^{-1}. The cloud downdraft mass flux is significant, noting it has a magnitude of about half of the updraft mass flux in the middle and lower troposphere during convective periods. This is similar to the result from the 7-day simulation during Phase III of GATE (Grabowski et al., 1996). A diagnostic study by Nitta (1978) also showed that the downdraft mass flux is about a half the updraft mass flux during Phase III of GATE.

3.6 Surface heat fluxes

The impact of cloud systems on the surface heat fluxes is a key issue in atmosphere-ocean coupling. In the CRM, the surface fluxes are calculated using the cloud-scale data at the level just above the surface (50 m) and the observed evolving SST data. By using the observed SST, only a one-way interaction between cloud systems and the ocean is considered; that is, there is no feedback of cloud-scale processes to ocean processes. Similar to the large-scale forcing issue, the evolving SST already includes the feedback from natural cloud systems (and all other relevant processes for that matter). The main issue is the consistency between model-generated fluxes and those deduced from observations.

In order to evaluate the accuracy of model-produced surface fluxes, the domain-averaged surface sensible and latent heat fluxes averaged over a 6-hour period are compared with the 6-hourly observed surface fluxes (Lin and Johnson, 1996b) in Figs. 7 and 8. The CRM reproduces the observed variations of the surface sensible and latent heat fluxes during the 39-day period, such as large fluxes during the strong convective period (e.g., 11-15 December and 20-24 December), large latent heat fluxes during the westerly wind burst period (e.g., 30 December-2 January), and small fluxes during the undisturbed period (e.g., 7-12 January). However, the model-produced surface fluxes show smaller time variability than the observed fluxes. For instance, standard deviations of the time evolution of the surface fluxes is 6.7 W m^{-2} (E0), 6.4 W m^{-2} (E1) and 7.3 W m^{-2} (observation) for the sensible flux and 44.6 W m^{-2} (E0), 42.3 W m^{-2} (E1) and 45.5 W m^{-2} (observation) for the latent flux. This could be indicative

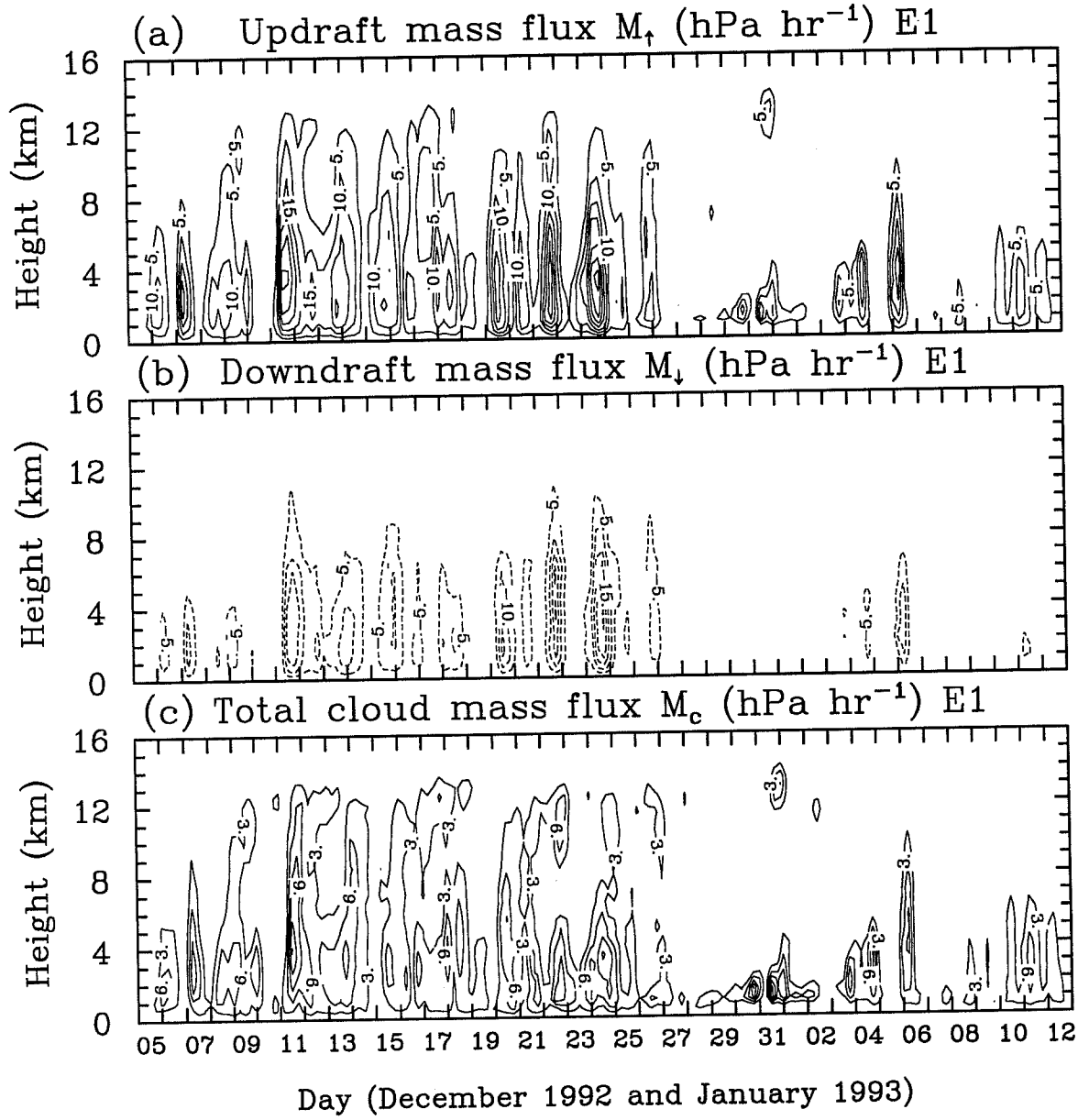

Figure 6: Evolution of the domain–averaged 6–hourly mean of the (a) updraft, (b) downdraft, and (c) total cloud mass fluxes calculated as explained in text. Contour interval is 5 hPa hr^{-1} for (a) and (b), and 3 hPa hr^{-1} for (c).

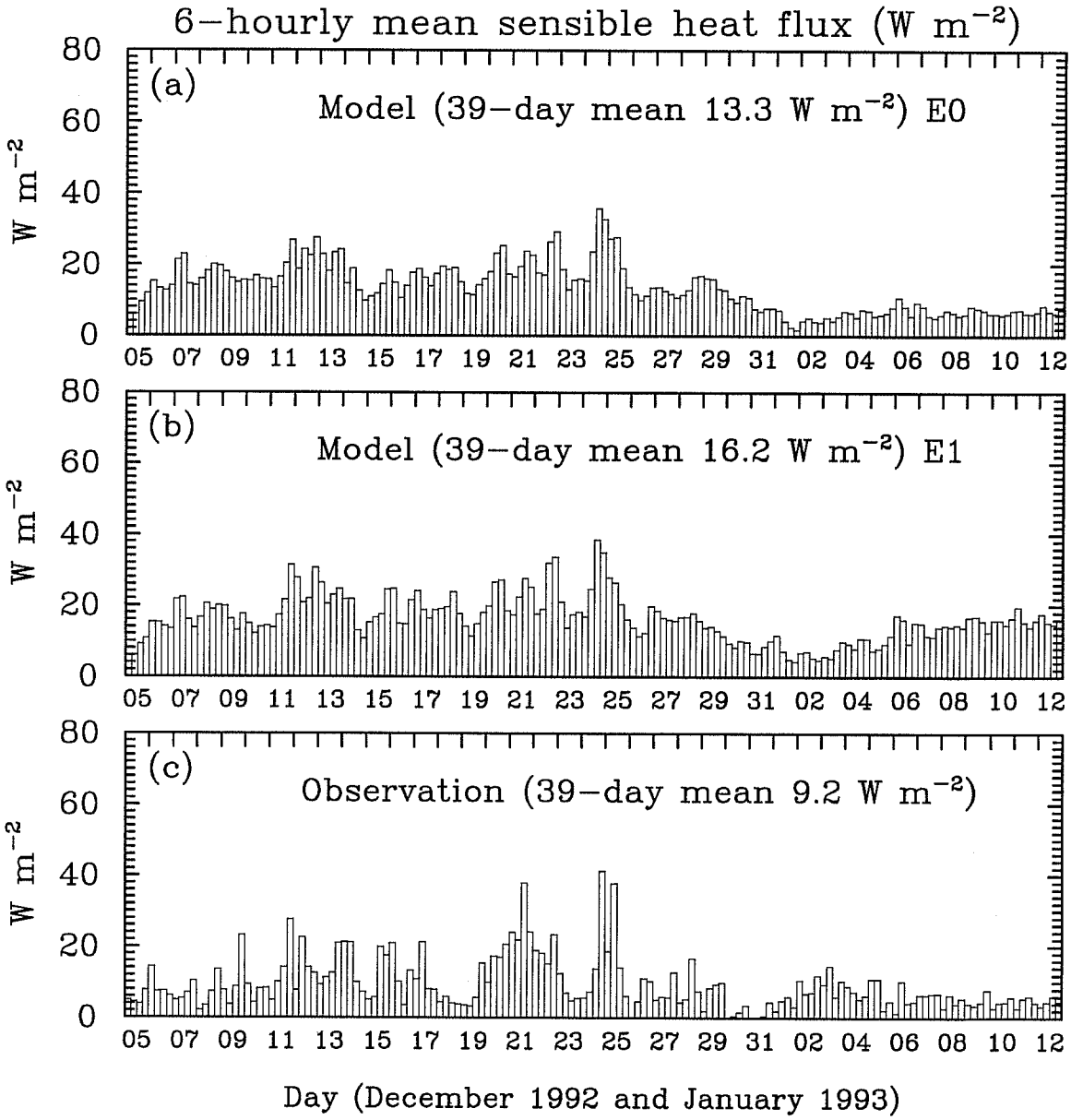

Figure 7: Evolution of the domain–averaged 6–hourly mean surface fluxes of sensible heat (W m^{-2}) from (a) the experiment E0, (b) the experiment E1, and (c) the TOGA buoy data, respectively.

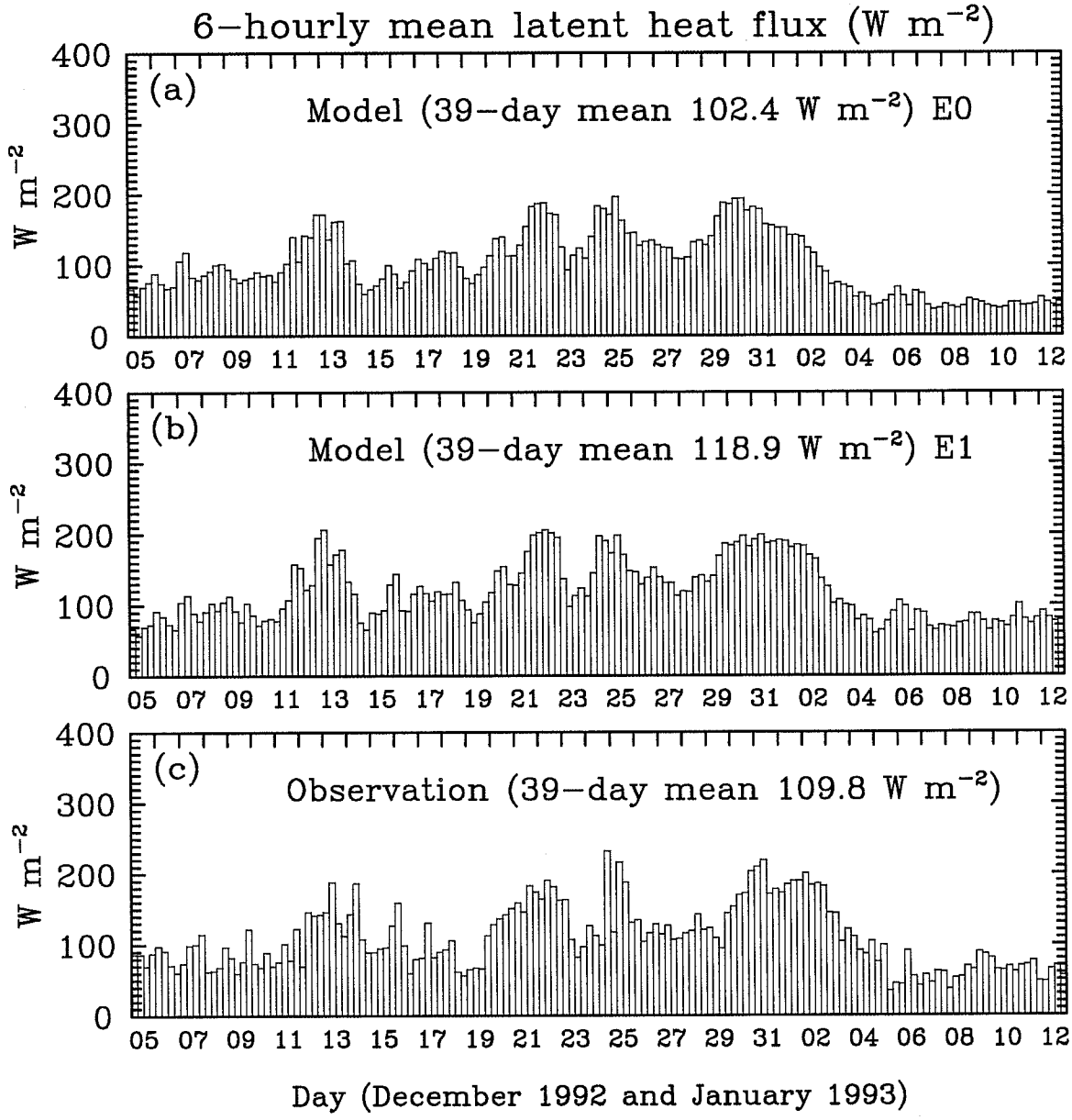

Figure 8: Same as Fig. 7 except for surface fluxes of latent heat.

of the restriction that only four buoys were used to obtain the observational data. Application of constant large-scale forcing over a 6-hour period in the CRM may also play a role.

The surface fluxes from the control experiment E0 are smaller than in the experiment E1. This is consistent with the enhanced moisture and temperature in the control experiment. The 39-day means of sensible and latent heat fluxes are 13.3 W m^{-2} and 102.4 W m^{-2} for the experiment E0, 16.2 W m^{-2} and 118.9 W m^{-2} for the experiment E1, and 9.2 W m^{-2} and 109.8 W m^{-2} for the observations, respectively. The larger sensible heat flux from the model compared with the sensible heat flux based on the buoy data is partly due to the large air-sea potential temperature difference between the ocean surface and the lowest model level (i.e., 50 m). Since the bulk formula developed for TOGA COARE is based on the potential temperature at height of 15 m, use of the lower potential temperature at 50 m in the bulk formula would lead to a larger vertical temperature gradient which, in turn, would lead to larger sensible heat fluxes.

3.7 Radiative fluxes

Evaluation of the model-produced data by the observations presented in the last section indicates that the cloud-scale fields generated by the CRM are basically trustworthy. This allows further analysis of the interaction of radiative fluxes with the atmosphere and the underlying ocean surface. The albedo and the outgoing longwave radiation (OLR) at the top of atmosphere are two quantities, derived from satellite measurements, that are important from the climate perspective. Albedo is the ratio of reflected shortwave radiative flux to the incoming solar heating at the top of atmosphere.

Figure 9 shows the evolution of the OLR from the model, from the FC data and from the GMS-4 satellite brightness temperature data, respectively. Model output (archived every 15 minutes) is averaged over the 900-km domain. The FC data is 3–hourly data with 2.5° horizontal resolution (Zhang et al., 1995; Rossow and Zhang, 1995). The GMS data is hourly data with 0.1° or 11 km horizontal resolution. Both the FC and GMS data are averaged over the IFA. The conversion of brightness temperature data to the broadband OLR data is performed using the narrowband-to-broadband transformation of Minnis and Harrison (1984). The experiments E0 (Fig. 9a) and E1 (Fig. 9b) produce similar time series of OLR during the 39-day simualtion, except during the periods 18-19 December and 7-12 January. The moisture unrealistically stored inside the domain (see Fig. 2) during these two periods, reduces the longwave flux escaping to space, so the OLR is smaller in E0 than in E1. The 39-day mean OLR is 179 W m^{-2} and 188 W m^{-2} for E0 and E1, respectively. The variation of OLR during the 39-day period is fairly similar comparing the model-produced OLR (Fig. 9b) with the observed OLR (Figs. 9c

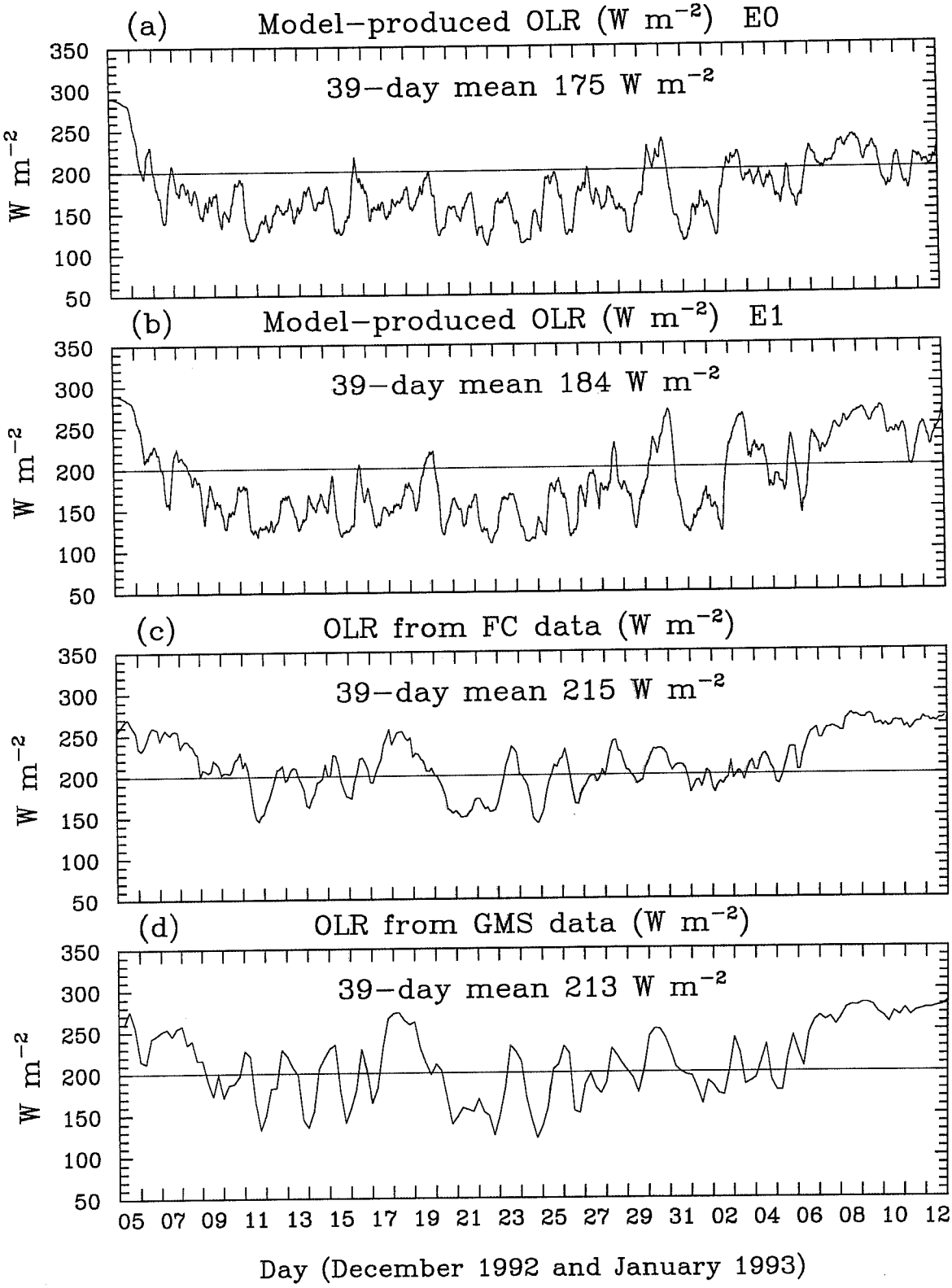

Figure 9: Evolution of OLR from (a) the experiment E0, (b) the experiment E1, (c) the Flux and Cloud data (3 hourly), and (d) the GMS data (6 hourly). Units are W m^{-2}.

and 9d). In strong convective events (e.g., 11-15 December and 20-24 December) the OLR is small (below 150 W m^{-2}), while during suppressed periods (e.g., 7-12 January) OLR is quite large (around 250 W m^{-2}). The 39-day mean OLR from experiment E1 is about 15 % off the observed values (215 W m^{-2} for the FC data and 213 W m^{-2} for the GMS data). This is consistent with the enhanced moisture still present for the E1 experiment despite the moisture relaxation technique.

The albedo comparison between the model and observation also shows reasonable agreement (Fig. 10). Only albedo data from the FC data are available. Both model-produced (Figs. 10a and 10b) and observed (Fig. 10c) albedo show that during convective periods (e.g., 11-15 December and 20-24 December) clouds reflect more shortwave flux and the domain-averaged albedo is large, while during clear sky periods (e.g., 7-12 January) less shortwave flux is reflected back to space and albedo is relatively small. The 39-day means are about the same, 0.43 for the experiment E0, 0.39 for the experiment E1, and 0.37 for the FC data. The smaller albedo for E1 compared to E0 is mainly due to the better control of upper tropospheric clouds due to the moisture relaxation technique.

4. THREE-DIMENSIONAL SIMULATIONS OF GATE CLOUD SYSTEMS

Largely due to the limitations of computer resources, most previous CRM studies adopted the 2D framework. However, the natural situation is clearly three dimensional. The long-standing questions remain to be answered are how cloud systems respond to the large-scale forcing with an extra degree of freedom in the 3D configuration, and how cloud properties and collective effects of cloud systems on the thermodynamic budgets, radiative fluxes and surface fluxes generated using 3D framework differ from those using 2D framework. Few 3D CRMs have been performed to answer these questions. Lipps and Hemler (1986) performed a set of 4-hour simulations of deep tropical convection using a cloud model with a horizontal domain (24km×16km) and a 500-m resolution. Tao and Soong (1986) and Tao et al. (1987) also performed several 3D simulations using a horizontal domain of 32km×32km with a 1-km resolution. In all these 3D simulations, the model domain is clearly too small for the development of cloud systems such as nonsquall cloud clusters and squall lines. Recognizing this limitation, two unprecedented 3D experiments (with and without the Coriolis force) are performed for a period of September 1 through September 7, 1974 during Phase III of GATE. A 7-day simulation of TOGA COARE cloud systems is currently underway. Some preliminary results from the 7-day GATE simulation without the Coriolis force will be presented in this section.

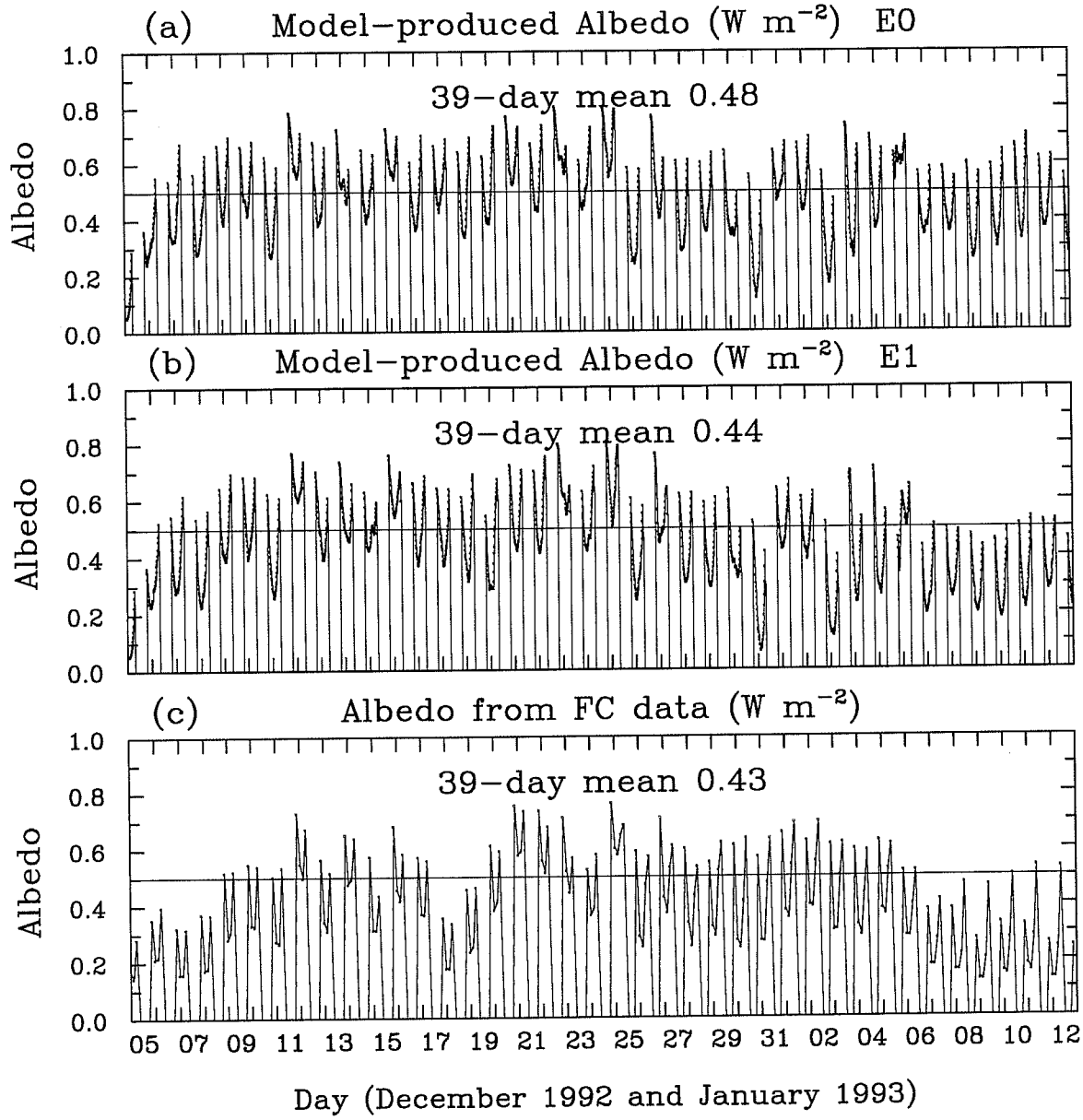

Figure 10: Evolution of albedo from (a) the experiment E0, (b) the experiment E1, and (c) the Flux and Cloud data.

4.1 Large-scale forcing and wind fields

The objectively-analyzed GATE Phase III dataset discussed in Esbensen et al. (1982) and Ooyama (1987) was used. The evolving large-scale profiles of temperature, moisture, winds and advective tendencies of temperature and moisture were averaged over the 3° × 3° array (i.e., 7-10°N and 22-25°W). A constant sea surface temperature of 27.2°C was used.

Figure 11 shows the evolution of the large-scale forcing for the temperature and water vapor mixing ratio, and the east-west wind component during the period 1-7 September 1974. The forcing is characterized by several episodes of cooling and moistening (days 2, 4, and 5) with the maximum cooling -15 K day^{-1} and moistening 3 g kg^{-1} day^{-1} on day 2 (Figs. 11a and 11b). The east-west wind component (Fig. 11c) features a strong easterly jet around 4 km. The associated low-tropospheric wind shear persists during days 3 and 4. Easterlies dominate in the upper troposphere. Toward the end of 7-day period (days 6 and 7), westerlies appear in the lower troposphere and at the surface. The north-south wind component (Fig. 11d) is characterized by the southerlies (northerlies) at lower levels and northerlies (southerlies) at upper levels during the period of days 1-5.

4.2 Preliminary analyses of 3D CRM data

Figure 12 presents three snapshots of the total condensate field (the sum of cloud water, ice water and rain water mixing ratio) from the 7-day simulation. Three different cloud systems, namely nonsquall cloud cluster, squall line and scattered convection are successfully reproduced by the CRM approach with the use of large domain. The nonsquall cluster develops under the strong large-scale forcing and weak low-level shear (day 2) and is characterized by a circular type of structure. Various types of clouds such as deep and shallow clouds, small cloud bands can be found in Fig. 12a. The squall line is reproduced under the moderate forcing and strong low-level wind shear (day 4), which was studied by many observational, numerical and theoretical studies (see Houze, 1993). The interesting features in Fig. 12b are the pronounced deep convection in the leading edge of the system, extensive anvil clouds (about 200 km wide) to the rear, and few deep and shallow clouds. Scattered convection is a response to the weak forcing condition (day 7) and has a southwest-northeast oriented line structure (Fig. 12c). The short line convection is mainly controlled by the low-level wind field (Figs. 12c and 12d). The qualitative comparison of these three cloud systems with the GATE radar composites (Fig. 13) shows overall similarities. The detail analyses of cloud properties using the CRM-produced 3D data are currently underway.

Figures 14 and 15 show the 7-day evolution of cloud mass fluxes produced by the 3D and 2D CRMs, respectively. The updraft and downdraft mass fluxes are averaged over the whole

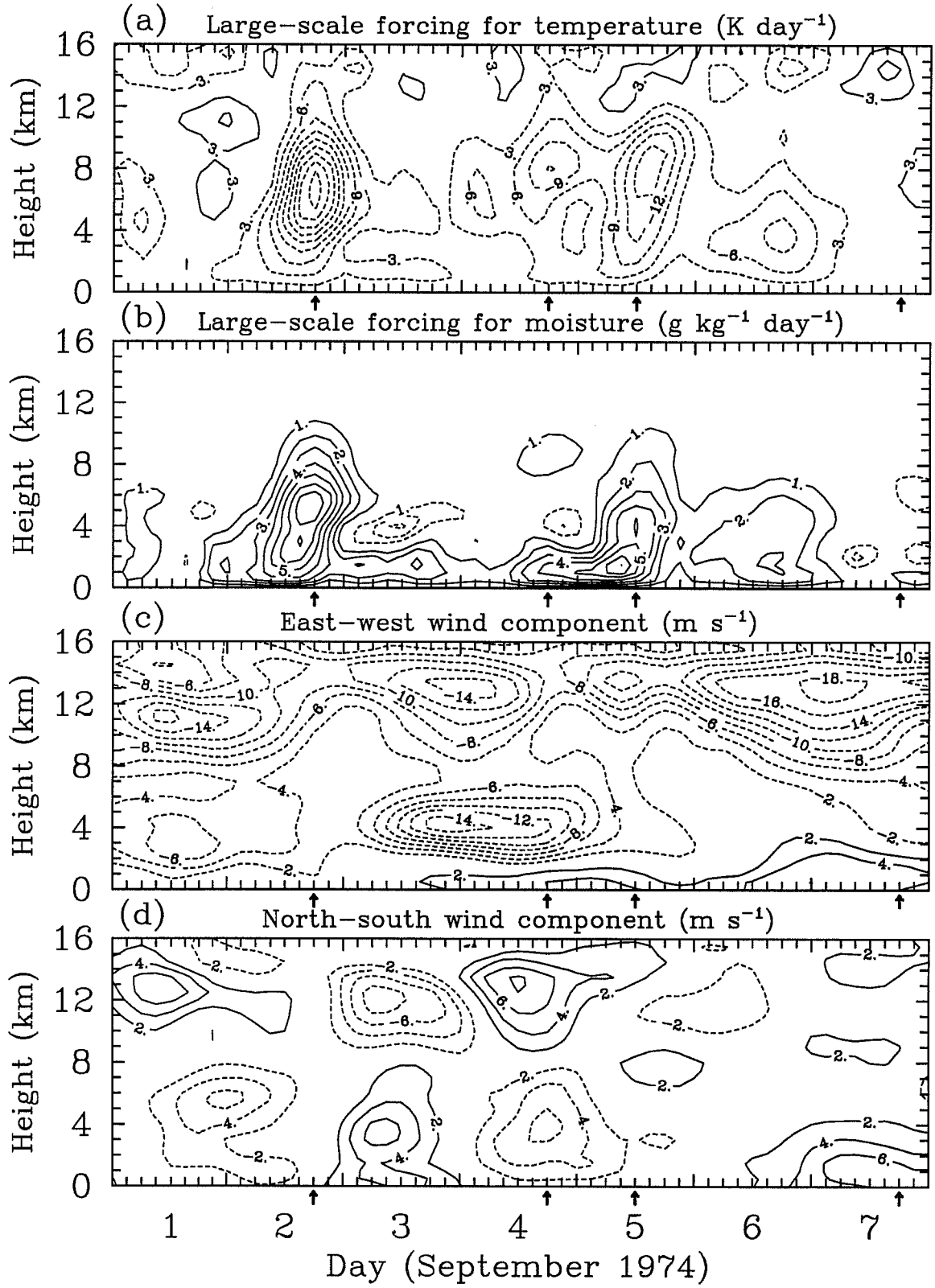

Figure 11: Evolution of the large-scale forcing for the temperature (panel a) and the water vapor mixing ratio (panel b), the east–west wind component (panel c), and the north-south wind component (panel d) averaged over the $3° \times 3°$ array of GATE. Contour intervals are 3 K day^{-1} in (a), 1 g kg^{-1} day^{-1} in (b), and 2 m s^{-1} in (c) and (d).

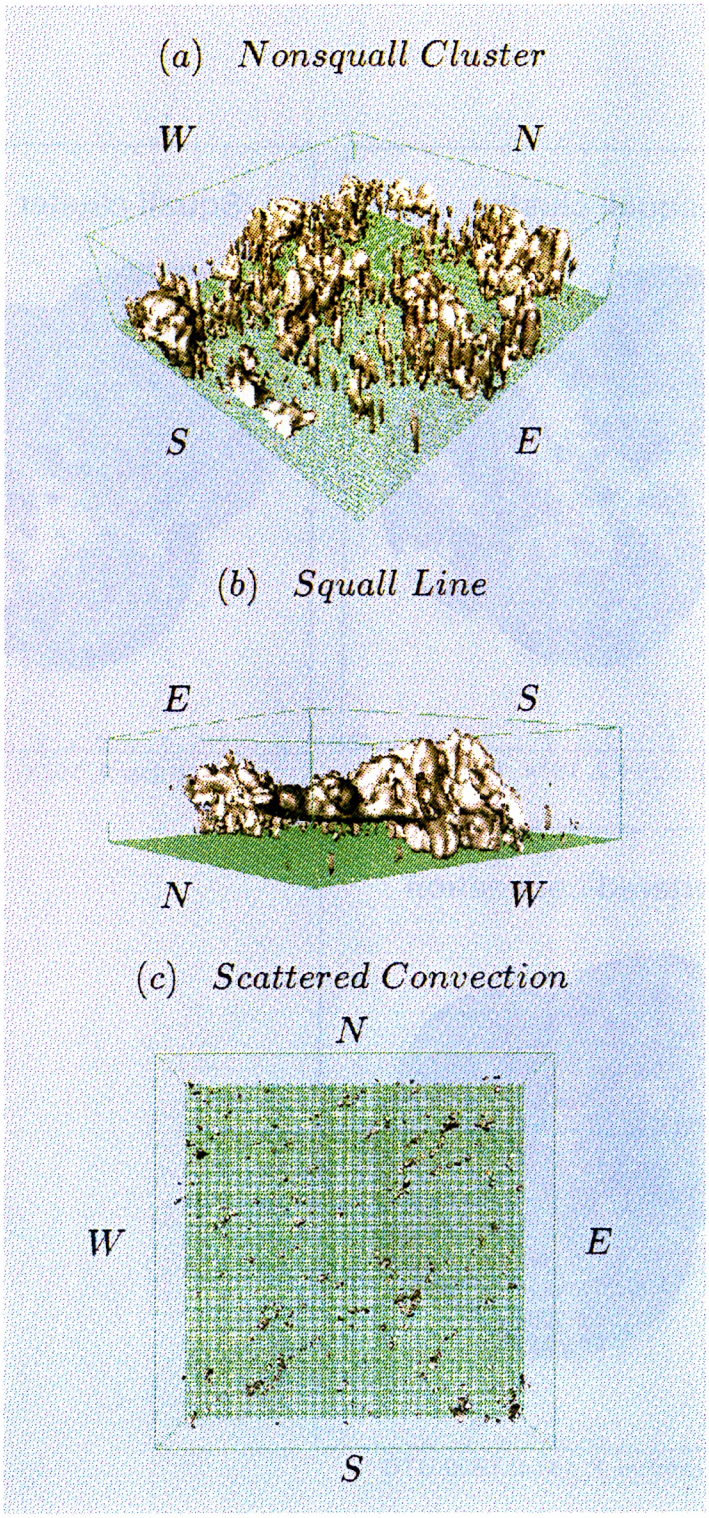

Figure 12: Snapshots of the total condensate field (with the isosurface of 0.1 g kg^{-1}) in a three-dimensional domain (400km×400km×26km) for (a) a nonsquall cloud cluster (South-east view, 2 September, 1974), (b) a squall line (North-west view, 4 September, 1974), and (c) scattered convection (top view, 7 September, 1974).

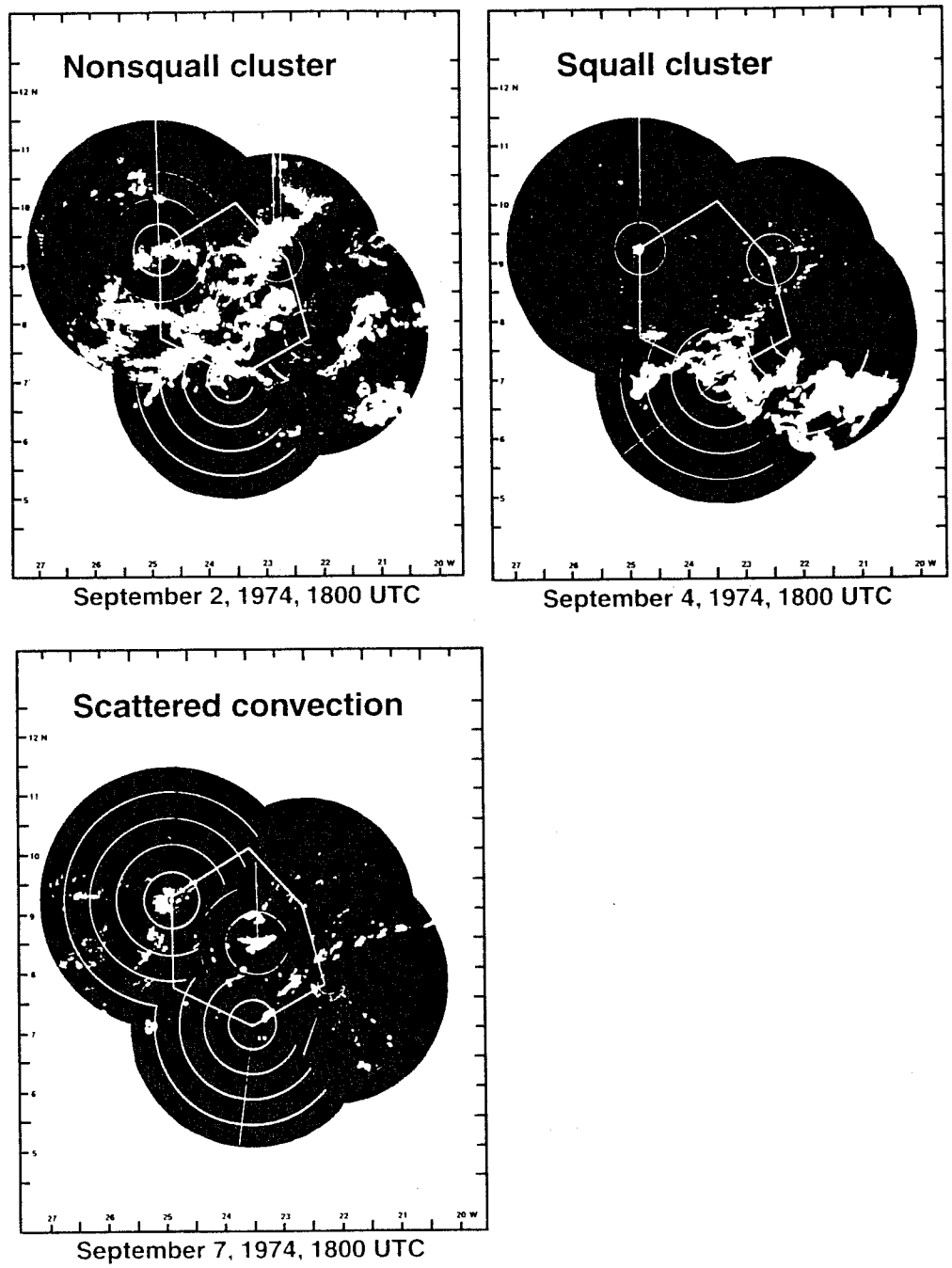

Figure 13: Radar echo composites for nonsquall clusters (2 September 2, 1800 UTC), a squall line (4 September, 1800 UTC), and scattered convection (7 September, 1800 UTC) from GATE International Meteorological Radar Atlas (Arkell and Hudlow 1977).

domain for the grid points with the total condensate larger than and equal to 0.1 g kg^{-1}. The total cloud mass flux is the sum of updraft and downdraft mass fluxes. The larger mass fluxes are consistent with the development of nonsquall clusters (days 2 and 5) and squall line (day 4), and the downdraft mass fluxes have a magnitude of about half of the updraft mass fluxes in both of 3D and 2D simulations. Comparing the 3D fluxes with the 2D fluxes, it is found that the updraft and downdraft mass fluxes from the 2D simulation are stronger than those from the 3D simulation when the easterly jet and the low-level wind shear are present (from day 3 to day 7) (Fig. 11c). The unrealistically large updraft and downdraft mass fluxes from the 2D simulation appear in the second half of day 3 and the first half of day 4 associated with the low-level easterly jet (Fig. 11c). But, the updraft and downdraft mass fluxes have similar magnitudes on day 2 for both the 3D and 2D simulations when the vertical wind shear is about zero below 8 km (Fig. 11c). This suggests that the response of cloud systems to the large-scale forcing is different under the 3D and 2D framework when dynamical factors such as the low-level wind shear are present. Recognizing the importance of cloud mass fluxes for the parameterization of cloud systems in the large-scale models, the cloud-radiation and cloud-surface interactions, the detail analyses are being performed to further understand the difference and similarity between the 3D and 2D simulations.

5. SUMMARY

The major points from this study can be summarized in the following:

* CRM approach that combines *evolving* large-scale observations with the cloud-scale model shows great potential for producing realizations of tropical cloud systems and realistic cloud-scale datasets. The model-produced data can be quantitatively evaluated against many independent data sources.

* The lack of large-scale advective tendency for the condensed water and the use of periodic lateral boundary conditions together result in the enhanced relative humidity in the upper troposphere. The interaction of extra moisture with the radiative processes produce the so-called greenhouse effect.

* The 3D simulation produces remarkably realistic cloud field evolutions. Both updraft and downdraft mass fluxes simulated using the 2D framework are stronger than those simulated using the 3D framework when the low-level vertical wind shear is present.

* The model-produced data can be used to improve convection parameterization schemes in GCMs and to study the cloud-radiation interaction, and this work is underway.

* The coupling of cloud-resolving models with ocean models can be used to quantify the effects of cloud systems and oceanic processes in the regulation of SST over the warm pool.

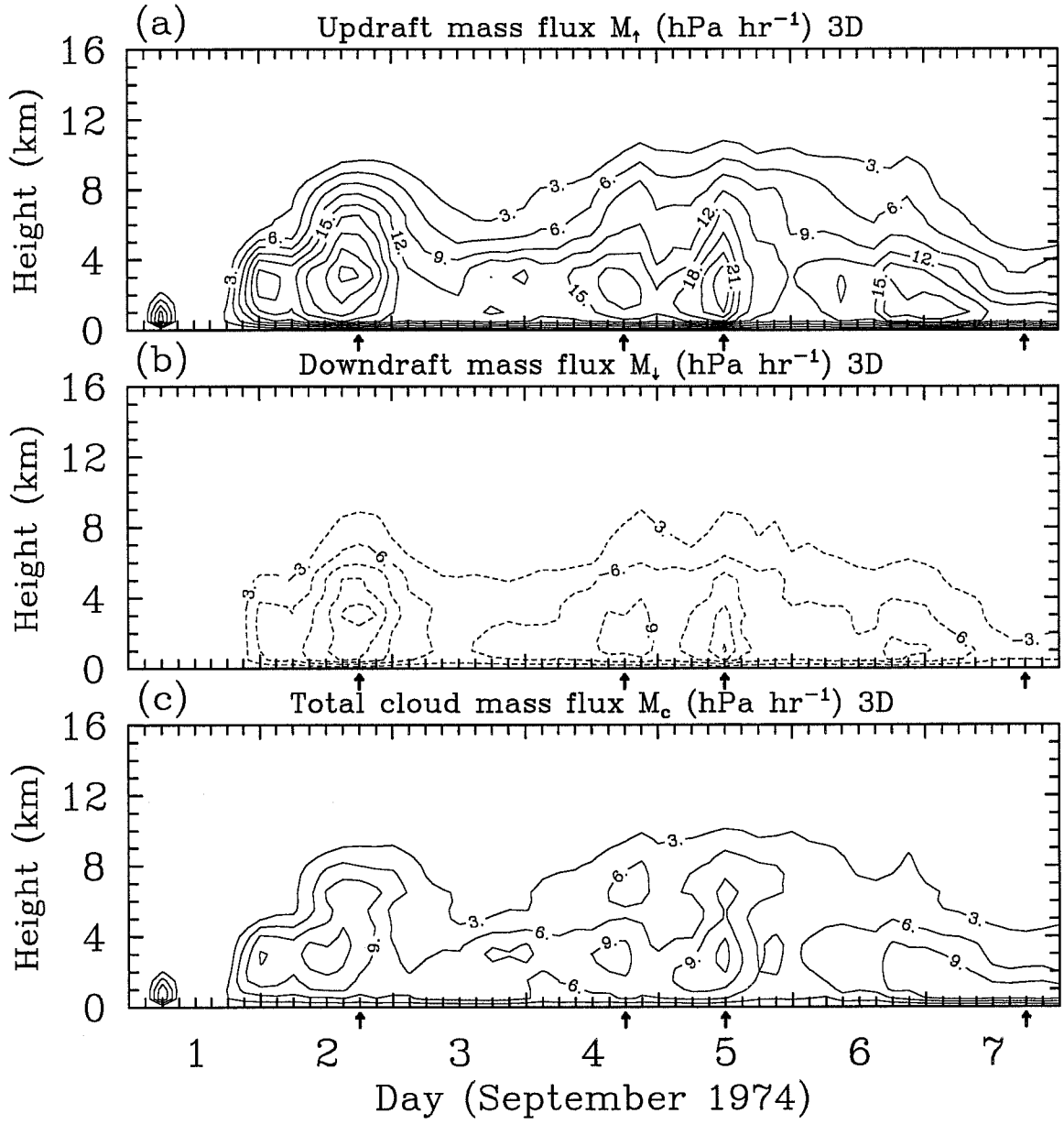

Figure 14: Evolution of the domain–averaged 3–hr mean of the updraft and downdraft mass fluxes and the total mass flux (panels a, b and c, respectively) for the 7-day period during GATE Phase III produced by the 3D CRM. Contour interval is 3 hPa hr^{-1}.

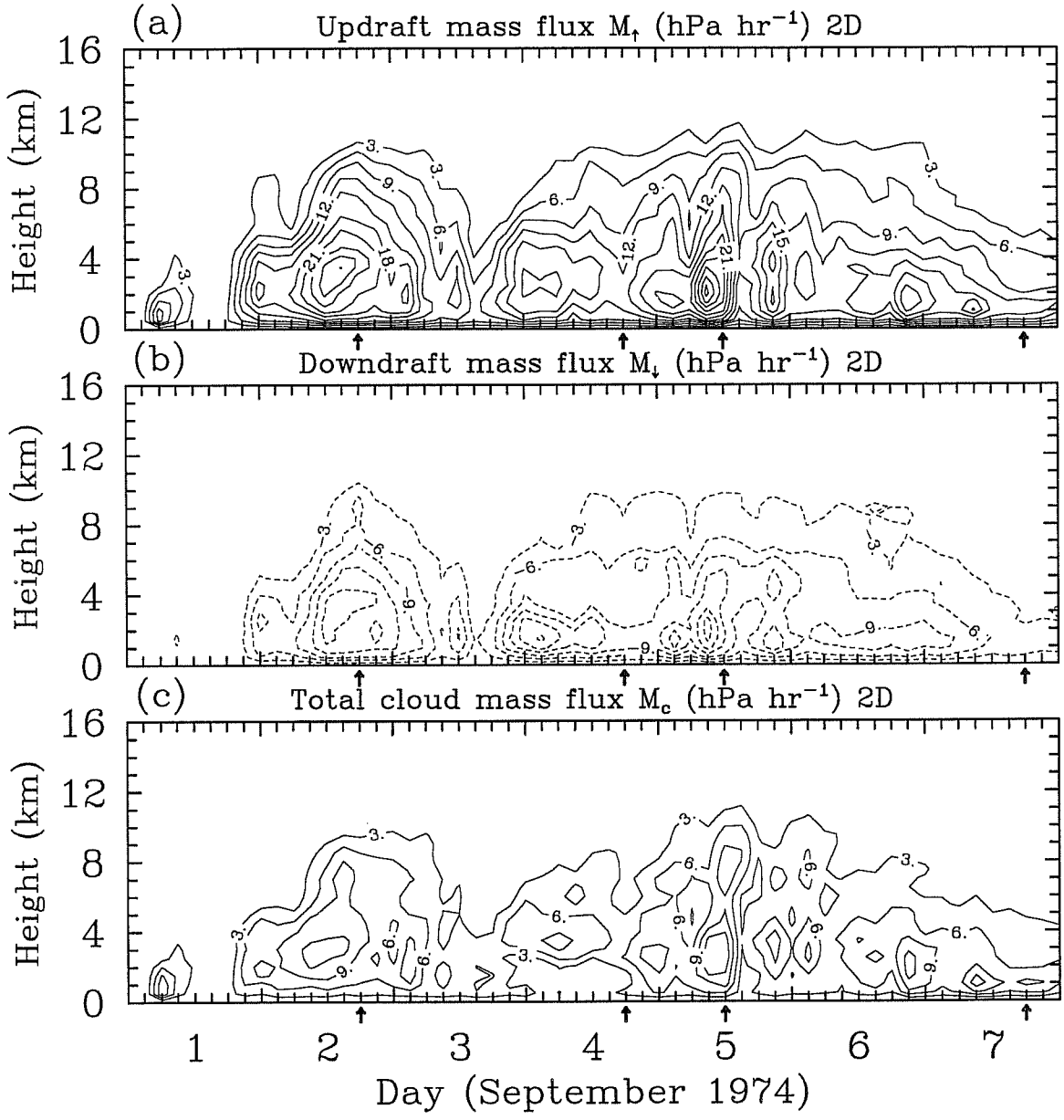

Figure 15: Same as Fig. 14 except by the 2D CRM.

ACKNOWLEGEMENTS

The authors greatly enjoy the collaboration with Wojtek Grabowski. The technical support of Bill Hall on the use of parallel code of Clark-Hall cloud model and Bill Anderson on reading observational datasets in different formats are gratefully acknowledged. The authors would like to thank Richard Johnson and Xin Lin (TOGA COARE IFA soundings and budgets), Bob Weller and Steven Anderson (IMET data), Michael McPhaden (TAO buoy data), Tetsuo Nakazawa (Japanese GMS-4 infrared data), and William Rossow and Yuan-Chong Zhang (FC data) for providing valuable data sets. Thanks also to Chris Fairall for providing the TOGA COARE bulk surface flux algorithm.

REFERENCES

Arkell, R., and M. Hudlow, 1977: *GATE International Meteorological Radar Atlas.* Environmental Data Service, NOAA, 222 pp. [Available from the Superintendent of Documents, U.S. Government Printing Office, Washington, D.C., 20402; Stock No. 003-019-00038-1.]

Browning, K. A., 1994: Survey of perceived priority issues in the parameterizations of cloud-related processes in GCMs. *Quart. J. Roy. Meteor. Soc.,* **120**, 483-487.

Cess, R. D., et al., 1989: Interpretation of cloud-climate feedback as produced by 14 atmospheric general circulation models. *Science,* **245**, 513-516.

Clark T. L., W. D. Hall, and J. L. Coen, 1996: Source code documentation for the Clark-Hall cloud-scale model: Code version G3CH01. NCAR Technical Note, NCAR/TN-426+STR. 137 pp. [Available from NCAR Information Service, P. O. Box 3000, Boulder, CO 80307.]

Esbensen, S. K., E. I. Tollerud, and J.-H. Chu, 1982: Cloud-cluster-scale circulations and the vorticity budget of synoptic-scale waves over the eastern Atlantic Intertropical Convergence Zone. *Mon. Wea. Rev.,* **110**, 1677-1692.

Fairall, C. W., E. F. Bradley, D. P. Rogers, J. B. Edson, and G. S. Young, 1996: Bulk parameterization of air-sea fluxes for Tropical Ocean-Global Atmosphere Coupled-Ocean Atmosphere Response Experiment. *J. Geophys. Res.,* **101**, 3747-3764.

Grabowski, W. W., X. Wu, and M. W. Moncrieff, 1996: Cloud resolving modeling of tropical cloud systems during Phase III of GATE. Part I: Two-dimensional experiments. *J. Atmos. Sci.,* **53**, 3684-3709.

Hall, W. D., and T. L. Clark, 1996: Parallel code development and application to the studies

of mechanically and wave-induced turbulence. *Preprints, 7th Workshop on the Use of Parallel Processors in Meteorology*, European Centre for Medium-Range Weather Forecasts, Reading, United Kingdom, December 2-6, 1996.

Houze, R. A., 1993: *Cloud Dynamics.* Academic Press, 570 pp.

Kessler, E., 1969: *On the distribution and continuity of water substance in atmospheric circulations.* Met. Monog. **10**, No. 32, 84 pp.

Kiehl, J. T., J. J. Hack, and B. P. Briegleb, 1994: The simulated Earth radiation budget of the National Center for Atmospheric Research community climate model CCM2 and comparisons with the Earth Radiation Budget Experiment (ERBE). *J. Geophys. Res.*, **99**, 20,815-20,827.

Koenig, L. R., and F. W. Murray, 1976: Ice-bearing cumulus cloud evolution: Numerical simulation and general comparison against observations. *J. Appl. Meteor.*, **15**, 747-762.

Lin X., and R. H. Johnson, 1996a: Kinematic and thermodynamic characteristics of the flow over the western pacific warm pool during TOGA COARE. *J. Atmos. Sci.*, **53**, 695-715.

—-, and —-, 1996b: Heating, moistening and rainfall over the western pacific warm pool during TOGA COARE. *J. Atmos. Sci.*, in press.

Lipps, F. B., and R. S. Hemler, 1986: Numerical simulation of deep tropical convection associated with large-scale convergence. *J. Atmos. Sci.*, **43**, 1796-1816.

Minnis, P., and E. F. Harrison, 1984: Diurnal variability of regional cloud and clear-sky radiative parameters derived from GOES data. Part III: November 1978 radiative parameters. *J. Climate Appl. Meteor.*, **23**, 1032-1051.

Moncrieff, M. W., et al., 1997: GEWEX Cloud System Study (GCSS) Working Group 4: Precipitating Convective Cloud Systems. *Bull. Amer. Meteor. Soc.*, May issue.

Nitta, T., 1978: A diagnostic study of interaction of cumulus updrafts and downdrafts with large-scale motions in GATE. *J. Meteor. Soc. Japan*, **56**, 232-242.

Ooyama, K., 1987: Scale-controlled objective analysis. *Mon. Wea. Rev.*, **115**, 2476–2506.

Rossow, W. B., and Y.–C. Zhang, 1995: Calculation of surface and top of atmosphere radiative fluxes from physical quantities based on ISCCP datasets, 2. Validation and first results. *J.*